



HAL
open science

Physicochemical and magnetic properties of functionalized lanthanide oxides with enhanced hydrophobicity

J. Kujawa, S. Al-Gharabli, G. Wrzeszcz, K. Knozowska, R. Lagzdins, E. Talik, A. Dzedzic, Patrick Loulergue, Anthony Szymczyk, W. Kujawski

► **To cite this version:**

J. Kujawa, S. Al-Gharabli, G. Wrzeszcz, K. Knozowska, R. Lagzdins, et al.. Physicochemical and magnetic properties of functionalized lanthanide oxides with enhanced hydrophobicity. *Applied Surface Science*, 2021, 542, pp.148563. 10.1016/j.apsusc.2020.148563 . hal-03103486

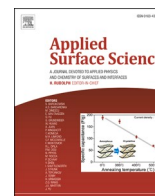
HAL Id: hal-03103486

<https://hal.science/hal-03103486>

Submitted on 25 May 2021

HAL is a multi-disciplinary open access archive for the deposit and dissemination of scientific research documents, whether they are published or not. The documents may come from teaching and research institutions in France or abroad, or from public or private research centers.

L'archive ouverte pluridisciplinaire **HAL**, est destinée au dépôt et à la diffusion de documents scientifiques de niveau recherche, publiés ou non, émanant des établissements d'enseignement et de recherche français ou étrangers, des laboratoires publics ou privés.



Full Length Article

Physicochemical and magnetic properties of functionalized lanthanide oxides with enhanced hydrophobicity

Joanna Kujawa^{a,*}, Samer Al-Gharabli^b, Grzegorz Wrzeszcz^a, Katarzyna Knozowska^a, Renars Lagzdins^{a,c}, Ewa Talik^d, Arkadiusz Dziezic^e, Patrick Loulergue^f, Anthony Szymczyk^f, Wojciech Kujawski^a

^a Faculty of Chemistry, Nicolaus Copernicus University in Toruń, 7 Gagarina Street, 87-100 Toruń, Poland

^b Pharmaceutical and Chemical Engineering Department, German Jordanian University, Amman 11180, Jordan

^c Faculty of Nature Sciences and Mathematics, Daugavpils University, 1 Parādes Street, Daugavpils LV-5401, Latvia

^d A. Chelkowski Institute of Physics, University of Silesia, Uniwersytecka 4, Katowice, Poland

^e Department of Conservative Dentistry with Endodontics, School of Medicine with the Division of Dentistry, Medical University of Silesia in Katowice, Pl. Akademicki 17, Bytom, Poland

^f Univ Rennes, CNRS, ISCR (Institut des Sciences Chimiques de Rennes) - UMR 6226, F-35000 Rennes, France



ARTICLE INFO

Keywords:

Lanthanide oxide
Functionalization
Physicochemistry
Superhydrophobicity
Petal and lotus effect

ABSTRACT

According to the developed bioinspired method in the one-step procedure, the material with the petal effect was switched to lotus one. Therefore, highly hydrophobic and super-hydrophobic materials with tunable adhesive properties and fractal-like structures were successfully produced with high efficiency (67–84%). The work's essence was to modify chemically selected powders of lanthanide oxides (CeO_2 , Pr_6O_{11} , Nd_2O_3 , and Gd_2O_3). High effectiveness of the functionalization process with 1H,1H,2H,2H-perfluorooctyltriethoxysilane (FC6) and n-octyltriethoxysilane (C6) was proven by various techniques, e.g. XPS, HR-TEM, ATR, XRD, zeta potential. Materials with water contact angle between 143.6° (CeO_2 -C6) and 175.5° (Nd_2O_3 -FC6) with thermally stable nanolayer (up to 380°C) were generated. Surfaces functionalized with FC6 possessed a polar component of surface free energy (SFE) close to zero. Water behavior in contact with the modified materials was studied, taking into consideration the unique electron structure of lanthanides assessed by goniometric measurement, also adhesion and spreading pressure were determined. Very low adhesion and polar SFE partly resulted in immediate bouncing of water droplet upon contact with the modified surface. The presented method allows preparing stable materials with a high potential in materials chemistry and modulation of surface features and engineering (e.g. heat transfer fluids, specific coating).

1. Introduction

Wettability is core to numerous biological processes, various industrial applications, and engineering technologies [1]. There is an overwhelming need to produce hydrophobic and superhydrophobic surfaces that are robust in difficult environments. The preparation of such materials will open the possibilities for new and advanced applications. Non-wetting surfaces, are often inspired by nature, and have attracted widespread consideration in surface engineering due to their extraordinary water repelling features. Depending on the final application, the surface can be as follows: superhydrophobic (lotus leaf) or superhydrophilic (fish scales) [2], superhydrophobic with high-adhesion

(Salvinia [3], petal rose [4]), and dry gecko foot [5]) or wet adhesion surfaces (tree frog foot [6]). There are many applications for the abovementioned surfaces, for example: droplet impact resistance [7], anti-corrosive surfaces [8], self-cleaning windows and walls [9,10], and low drag microfluidic channels [11,12] or anti-icing surface [13]. However, the implementation of non-wetting materials on a large scale or in industrial applications has been vulnerable due to synthesis techniques, which are not straightforwardly scalable, and the limited resistance to wear of these surfaces as well as their long-term stability. So far, superhydrophobic materials generated by a combination of surface topography and chemistry modifications have attracted significant attention of researchers and engineers [14,15]. To fabricate interfacial

* Corresponding author.

E-mail address: joanna.kujawa@umk.pl (J. Kujawa).

<https://doi.org/10.1016/j.apsusc.2020.148563>

Received 5 September 2020; Received in revised form 3 November 2020; Accepted 19 November 2020

Available online 25 November 2020

0169-4332/© 2020 The Authors.

Published by Elsevier B.V. This is an open access article under the CC BY-NC-ND license

(<http://creativecommons.org/licenses/by-nc-nd/4.0/>).

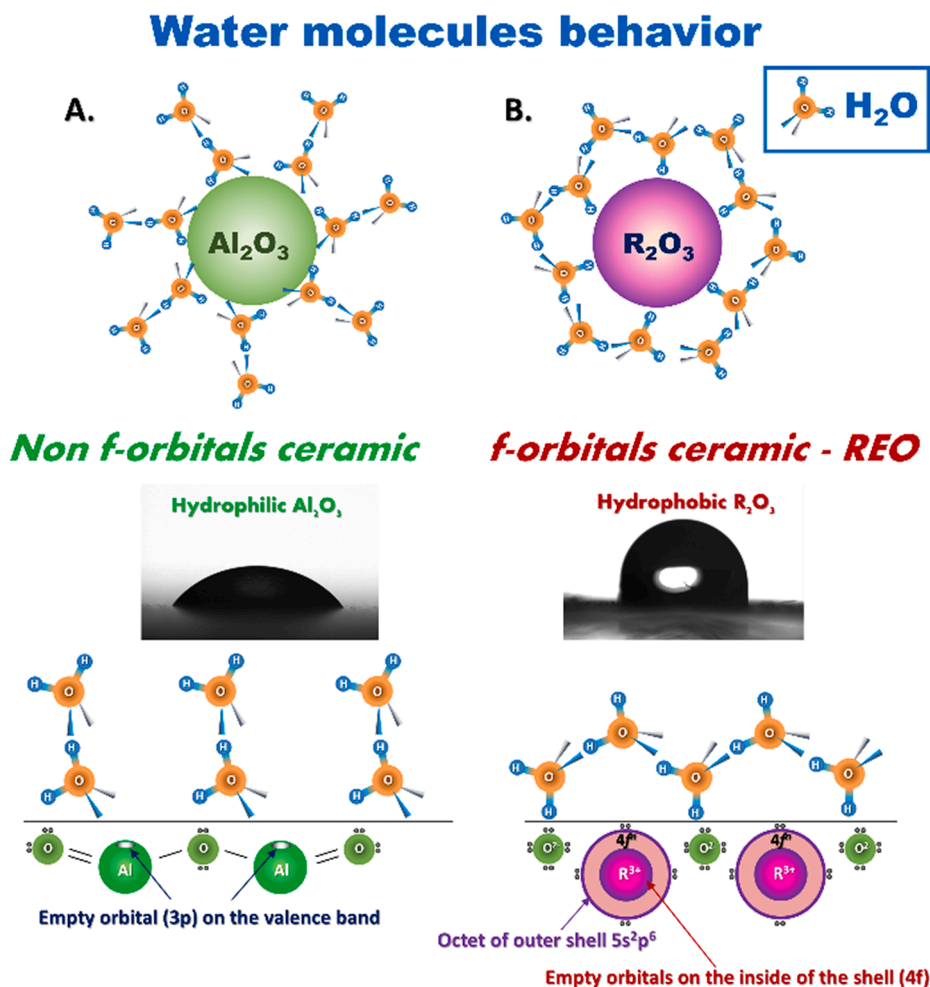


Fig. 1. Water molecules behavior on the ceramic surface of Al₂O₃ (an example of non-f-orbital ceramics) and R₂O₃ (example of f-orbital ceramics - REO) and the related wetting features of the surfaces.

materials with superwettability, a coating or chemical functionalization within the texture is implemented in micro or nanoscale. For instance, such a process can be accomplished on the naturally hydrophilic surface by chemical attachment of modifiers having hydrophobic nature and low surface energy, e.g. organosilanes [16,17], thiols [18] or introducing a texture to the material [1,19,20]. Even though the naturally hydrophilic materials e.g., ceramics or metal, possessing high surface energy can be turned to hydrophobic ones by modification with polymeric agents, these deteriorate in a harsh environment [14,21,22]. The disadvantage related to the use of polymeric modifiers is mostly related to chemical and/or thermal decomposition of the polymer and mechanical damage of the surface due to the reduced resistance of the grafted layer to high temperature and abrasion [15,18,22]. Recent research has demonstrated that a class of ceramics involving lanthanides, rare earth oxide (REO) ceramics, is intrinsically hydrophobic [21,23–25]. Moreover, REO ceramics are hard and mechanically highly stable, even after extreme processing conditions. Therefore, lanthanide oxides maintain their hydrophobic character e.g. under abrasive wear and exposure to high temperature (up to 1000 °C), as well as steam [26–28]. Their natural hydrophobicity is associated with their unique electronic structure that prevents hydrogen bonding with water molecules. That phenomenon arises from the shielding of unfilled 4f orbitals by the full octet of electrons in the outer shell (5s²p⁶), causing the protection of REO interactions from surrounding environment [21–25,29] (Fig. 1).

The description of the hydrophobicity mechanism for rare earth oxides is currently subject to discussions. Azimi and co-workers [23,24]

mentioned that roughness and surface chemistry plays the most critical role in the determination of REO wettability. This feature of the material is crucial if the modification process is to be taken into account. The modification process of REO surface e.g., by sputtering [23], electrodeposition [25], or atomic layer deposition [26] will cause variations in the metal-oxygen lattices. For instance, the increase of lattice oxygen sites corresponding to the rare-earth metal sites will affect the hydrophobicity of the material [30]. The above-mentioned phenomenon will increase the opportunities for generating new hydrogen bonding with interfacial water, which subsequently crumbles the structure of hydrophobic hydration, thereby increasing wettability.

The wettability of a material is directly associated with interfacial water [24,31]. Furthermore, to determine the wetting ability of the material, surface polarity and water-molecules orientation also need to be considered [30,32]. Tam et al. [30] pointed out that in the case of REO wetting feature, the relation between water contact angle (CA), crystallographic orientation, and surface energy (SE) needs to be evaluated. These authors studied 3 types of epitaxial REO films having the following orientation: (001), (110), and (111) and different surface energies. It was found that the water contact angle on those surfaces strongly depends on the crystallographic orientation. The highest CA was found for (111) surfaces, the lowest one, for (001) ones. That phenomenon was related to the surface energy, which was inversely proportional to CA [30]. The O-RE-O-terminated REO surface, according to Tam et al. [30] should demonstrate neutral charge due to the compensation of positive (δ^+) REⁿ⁺ ions and negatively charged ones (δ^-) O²⁻. Consequently, the attraction between surface and water

molecules is less likely, as the electrostatic force would not affect the O-RE-O-terminated surface owing to its charge-neutral surface. On the contrary, a surface with the following structure O-/RE-terminated REO should be positively or negatively charged with a dipole moment vertical to the surface that strongly attracts molecules with polar character e.g. water. Consequently, it was expected that the O-RE-O-terminated REO surface should demonstrate higher value of water contact angle than an O-terminated surface. The above-mentioned variations were related to the alterations in surface energy between the investigated orientations [30].

Oh and co-workers [26] have shown that, besides contact angle and surface energy, hygroscopic feature, and electronegativity influence the hydrophobicity of the material. Lundy et al. [33] have demonstrated that the surface hydroxylation degree significantly influences the water contact angle and its hysteresis. It was pointed out that the rise in water contact angle is caused by a decrease in the surface oxidation state. The study was performed for cerium oxide (CeO₂). The conclusion was that high atomic number of metal oxides capable of strongly adsorbing volatile species might signify a workable paradigm for obtaining robust surface coatings. Li and co-workers made [34] a suggestion to generate a superhydrophobic surface by application of plasma spray-vapor deposition. Samaria-doped ceria was used as an example of intrinsically hydrophobic material (contact angle 110°). The authors also investigated the impact of surface free energy on hydrophobicity. For this purpose, the chemical modification with stearic acid and 1,1,2,2-tetrahydroperfluorodecyltrimethoxysilane, as examples of low surface free energy modifiers, was performed. The generated surfaces had a stable hydrophobic layer after the coating process with the contact angle equal to 148° and 154° after treatment with stearic acid and 1,1,2,2-tetrahydroperfluorodecyltrimethoxysilane, respectively.

Due to the growing interest in generating new hybrid polymeric-based materials with different ceramic fillers [35–37], we introduced a new group of highly stable and fascinating ceramic fillers in the study reported here. Based on the literature survey, the research gap was identified and fulfilled by the presented work. Lack of highly stable ceramic materials with hydrophobic features maintained even after application in harsh conditions was pointed out. Taking into account the above-mentioned requirements, the aim of the work was defined, and materials with high stability and prolonged application were generated by one-step functionalization of selected lanthanide oxides. Moreover, the goal of the research was to characterize the produced materials systematically. The study of the REO's material features before and after functionalization has been performed.

2. Experimental part

2.1. Materials

Lanthanide oxides: cerium (IV) oxide (CeO₂), gadolinium (III) oxide (Gd₂O₃), praseodymium (III,IV) oxide (Pr₆O₁₁), and neodymium (III) oxide (Nd₂O₃) and modifiers: 1H,1H,2H,2H-perfluorooctyltriethoxysilane (CAS: 51851-37-7) labeled as FC6; n-octyltriethoxysilane (CAS: 2943-75-1) labeled as C6 were purchased from Abcr Chemicals (Germany). Glycerin, diiodomethane, chloroform (stabilized by 1% ethanol) were bought from Avantor Performance Materials Poland S.A (Poland) and used as received without further purification.

2.2. Scientific equipment

2.2.1. Material features – Morphology and chemistry

Attenuated total reflection - Fourier transform infrared spectroscopy (ATR-FTIR) was used to evaluate the efficiency of material surface functionalization. Bruker Vertex 80v ATR-FTIR apparatus with diamond crystal was applied. The resolution of 4 cm⁻¹, and 256 scans was used. Samples were analyzed in a powder form directly.

X-ray photoelectron spectroscopy (XPS) spectra were collected with

monochromatic Al K α radiation (1486.6 eV) at room temperature, using a PHI 5700/660 ESCA spectrometer (Physical Electronics, Lake Drive East, Chanhassen, MN, USA). The measurements were accomplished under the following conditions: ultra-high vacuum (UHV), take-off angle of 45°, the irradiated surface area of 0.8–2 mm, Al K α 1 monochromatic X-ray source (1486.6 eV), the energy resolution of approximately 0.3 eV; electron gun compensating positive surface charge (usually appearing for insulators) was also used. The C 1s component at 285 eV was used as the binding energy (BE) reference.

High-Resolution Transmission Electron Microscopy (HR-TEM) was performed using Tecnai G2 F20 X-Twin (FEI Europe), applying the accelerating voltage of 200 kV. TEM with HAADF high-angle annular dark-field and bright field imaging was implemented for the characterization of the modification process.

The X-ray diffraction (XRD) technique was used to determine the phase composition of REO materials. The spectra were collected in the 2 θ range of 5° – 90°, at room temperature, with an 0.02° step and the rate of 3°/min, using a Philips X'Pert PW 3040/60 diffractometer (Germany) with K α = 1.5418 Å and Cu lamp with 30 mA and 40 kV power. Rachinger's method with K α 2/K α 1 correction was employed.

Litesizer 500 (Anton Paar, Austria) was used for determining particle size and zeta potential. The stock dispersion of REO was performed in deionized water (18 M Ω cm) at a concentration of 1.5 mg/mL. Prior to the analysis, samples were dispersed with ultrasounds for 5 min and then directly diluted to the final concentration (100 μ g/mL) and analyzed. DLS (dynamic light scattering) and zeta potential were measured at 25 °C in deionized water (pH 5.8). The general-purpose model was used due to the low conductivity of the samples. Smoluchowski approximation has been used to convert the electrophoretic mobility into zeta potential.

Nitrogen adsorption/desorption analysis (ASAP 20120) was performed for the evaluation of pore size distribution and pore size of the tested ceramic powders (pristine and modified). Pore size and specific surface area of the REO material were studied by using BJH (Barrett-Joyner-Halenda) and BET (Brunauer–Emmett–Teller) models. Before analysis, each sample was degassed at 110 °C for 6 h.

Scanning electron microscopy (SEM) was performed using Quantax 200 equipped with an XFlash 4010 detector from Bruker AXS (Czech Republic). Before SEM analysis, the samples were sputtered with a gold nanolayer (Au, layer thickness 5 nm) to enhance the sample conductivity.

Thermogravimetric analysis (TGA), differential thermal analysis (DTA), and derivative thermogravimetry (DTG) were performed at the temperature range of 25–1100 °C, with a heating rate of 20 °C/min under nitrogen, applying Jupiter STA 449 F5 (Netzsch, Germany). The thermal resistance and sample stability were defined according to TGA and DTG. DTA provides the data related to changes in the energy of materials (enthalpy of the reaction and specific heat capacity). TGA was also used to determine the effectiveness of functionalization according to the method developed and described elsewhere [38,39].

2.2.2. Wettability study

Goniometer Attention Theta (Biolin Scientific, Gothenburg, Sweden) was used during material characterization experiments for the determination of contact angle. A thin film of powder was prepared on the microscopic glass for goniometric measurements with 3 μ l volume of testing liquid (water, glycerin, diiodomethane). The contact angle was measured three times, and the average value was presented. The determined contact angles values were used for the calculation of surface free energy (SFE) and its polar and dispersive components, according to the model developed by Owens, Wendt, Rabel, and Kaelble (OWRB) [40].

2.2.3. Magnetic properties

Electron paramagnetic resonance (EPR) was implemented for the characterization of magnetic features of ceramic materials before and

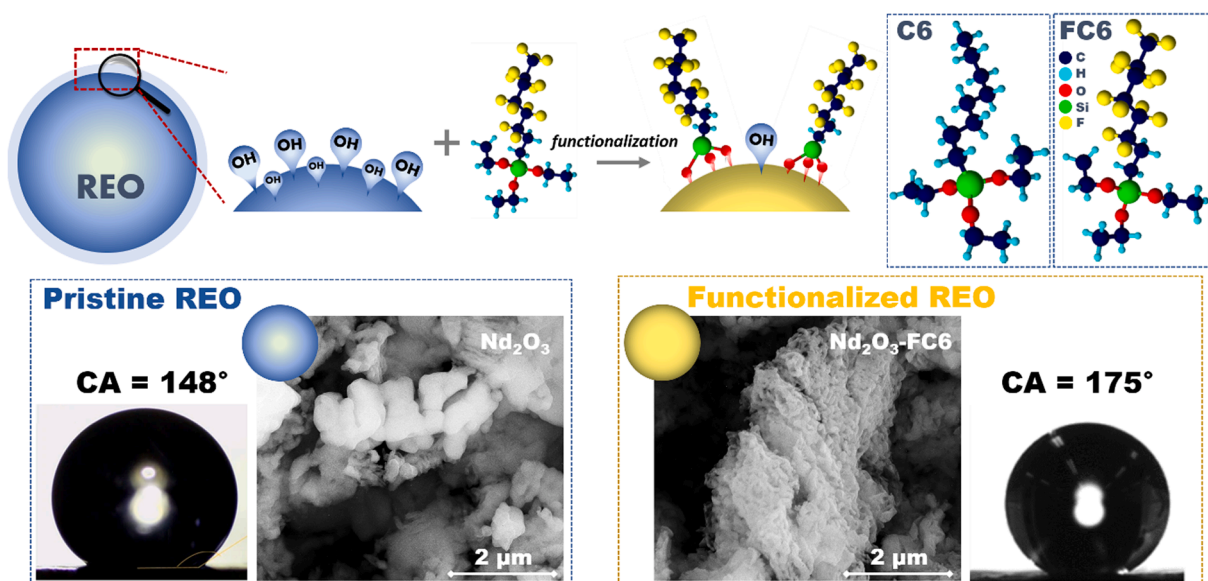


Fig. 2. Scheme of functionalization of REO – rare earth oxide (Nd_2O_3 as an example) with C6 or FC6 modifiers.

after functionalization. EPR spectra of the REO pristine and modified samples were recorded at room temperature with an X band (ca. 9.3 GHz) Radiopan EPR SE/X-2541M spectrometer with a 100 kHz modulation. To monitor the microwave frequency, a frequency meter was employed. The magnetic field was measured with an automatic NMR-type JTM-147 magnetometer.

2.3. Functionalization process

Prior to the modification process (Fig. 2), the pre-treatment step of rinsing each powder consecutively in the following solvents: acetone, ethanol, and distilled water was performed, as well as drying at 110 °C overnight. All lanthanide oxides were stored in a desiccator to maintain a constant temperature and humidity conditions. The 0.05 M grafting solutions of 1H,1H,2H,2H-perfluorooctyltriethoxysilane and *n*-octyltriethoxysilane were prepared in chloroform. The single grafting step consisted of adding an exact volume of modifier solution (7.5 ml) to a given amount of the lanthanide oxide powder (5 g). The ratio of modifiers (in mmol) to the mass of rare earth oxide (in g) was expressed as *Q* parameter (0.75 mmol g^{-1}) (Eq. (1)), it was the same for all investigated samples. The preparation of grafting solution, as well as the functionalization process, were performed at room temperature under an ambient atmosphere of nitrogen in a glovebox to avoid the risk of polycondensation of the modifiers. Grafting time was 5 h. All modifications were done in glass vials (20 ml) bolted with PTFE/butyl septa, placed on roller mixer (Stuart SRT6D, Bibby Scientific Limited, UK) to provide complete contact of samples with the modifier. Once the grafting process was finalized, the grafted samples were rinsed successively in ethanol, acetone, and distilled water, and dried at 90 °C overnight. The modified samples were subsequently characterized using various techniques.

$$Q_{\text{REO}} = \frac{\text{amount of modifier (C6 or FC6)}}{\text{REO mass}} \left[\frac{\text{mmol}}{\text{g}} \right] \quad (1)$$

3. Results and discussion

3.1. Functionalization efficiency

The efficiency of the functionalization process has been proven and studied by various analytical techniques. The goal of the modification process is to develop materials with superhydrophobic and low-adhesion features (lotus leaf effect), starting from hydrophobic

materials possessing highly adhesive properties (petal effect).

Spectroscopic methods, ATR-FTIR, and XPS proved that molecules used for grafting were covalently attached to the surface of REO oxides. In Fig. 3 and Fig. S1, the characteristic bands obtained in oscillating spectroscopy are shown. The bands located below 1000 cm^{-1} are ascribed to oxide. The broadband region around 3260 cm^{-1} is related to the intermolecular or intramolecular hydrogen bond of OH, particularly visible in Fig. 3B and S1A for Gd_2O_3 and CeO_2 samples. It is known from the literature [34,41] that oxide ions with large lattices, i.e., REO existing on the surface, are in Lewis base form, which will withdraw protons from water molecules to form hydroxyl groups when they are exposed to water molecules. The existence of the Si-O-X (X = REO) connection at the frequency of around 1000 cm^{-1} is associated with the chemical reaction between reactive groups of modifiers (i.e., ethoxy groups) and hydroxyls available on the REO surface.

The occurrence of characteristic vibration bands (Fig. 3, Fig. S1) of alkylsilanes in the region of $1550\text{--}950 \text{ cm}^{-1}$ is a consequence of the functionalization process (Fig. 2) [42]. The bands of the perfluorinated chains related to modification by FC6 molecules are seen at the frequency range of $1260\text{--}1018 \text{ cm}^{-1}$, in asymmetric (1250 cm^{-1}), and symmetric (1180 cm^{-1}) stretching mode of CF_2 functional group of FC6. The vibration of the Si-O-modifier bond is detected at the frequency of ca. 1510 cm^{-1} . During the functionalization with non-fluorinated compounds (C6), the bands at the frequency of 2850 cm^{-1} and 2920 cm^{-1} were observed and assigned to asymmetric and symmetric CH_2 stretching vibrations of the alkyl chain. Asymmetric vibration bands of CH_3 (1462 cm^{-1}) and CH_2 with in-plane deformation (1446 cm^{-1}) were found for functionalized materials with C6. Moreover, bands found at 1120 cm^{-1} and 1245 cm^{-1} , with different intensity, were related to the C-C-C stretching symmetric vibrations. On the basis of the data collected, it can be stated that the functionalization process was performed successfully.

Additionally, the confirmation of functionalization was assessed by XPS and HR-TEM analyses. The wide range of XPS spectrum of the selected pristine and functionalized REO – Nd_2O_3 has been presented in Fig. 4. XPS survey spectra of other ceramic materials are in Figs. S2-S4. On the pristine REO material, the core lines (e.g., Nd3d, Nd4d) and Auger electrons were visible (e.g., O KLL). However, as a result of the functionalization process with C6 and FC6, the core lines of C1s and F1s were detected, respectively. The most important finding has been that the functionalization process does not change the main features of the material and maintains its robustness. The complex shape of the lines for

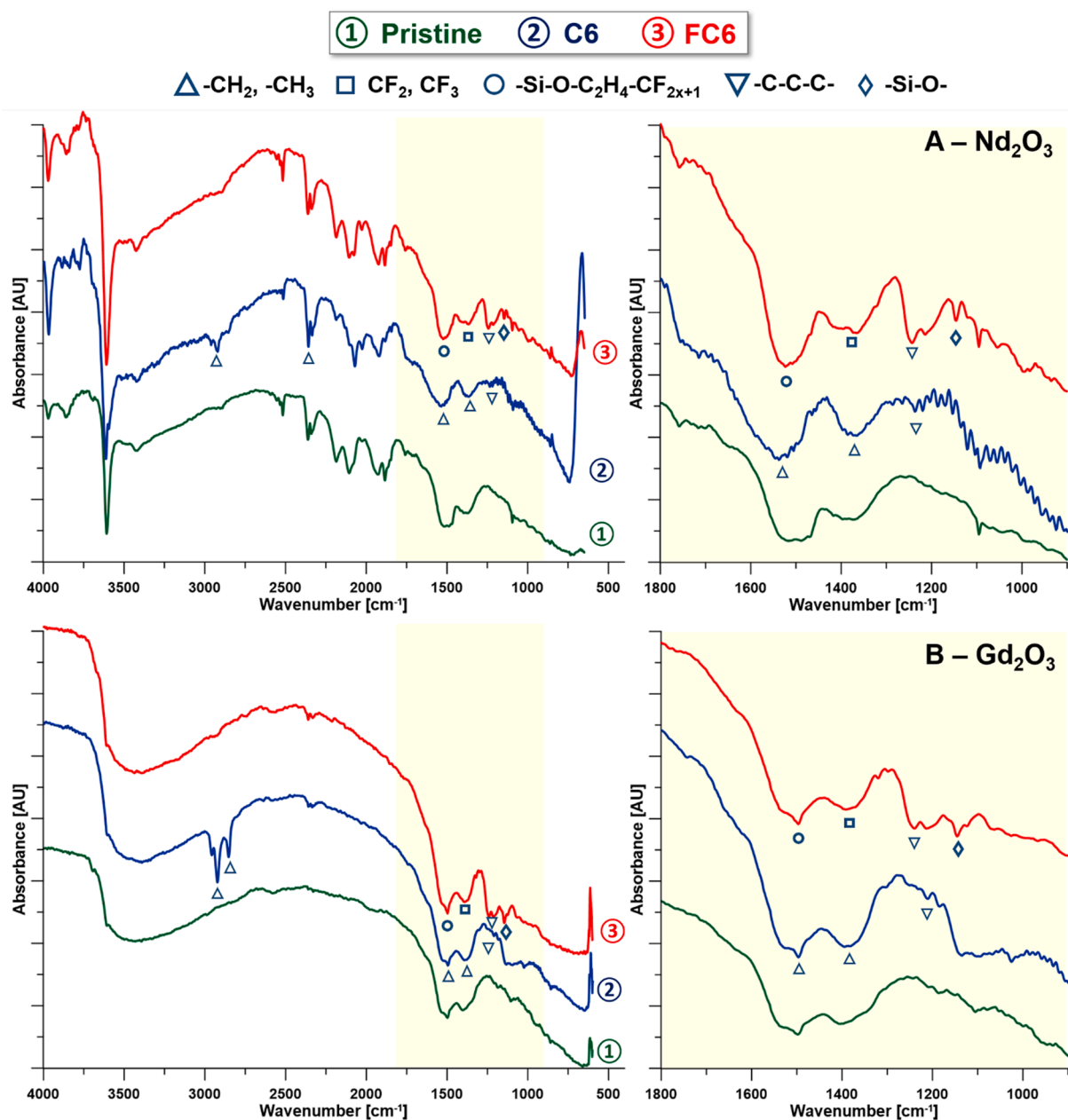


Fig. 3. ATR-FTIR spectra of pristine and functionalized REO materials, (A) Nd_2O_3 and (B) Gd_2O_3 .

REO originates from the simultaneous effect of solid-state hybridization and intra-atomic electrostatic coupling between 3d hole and outer unpaired 4f electrons [43]. The $\text{Nd}3d_{3/2}$ and $3d_{5/2}$ lines are split due to final state configurations of $3d^9 4f^4 L$ (L-hole on the $\text{O}2p$ valence band) on the low binding energy side and of the $3d^9 4f^3$ on the high energy side. The $\text{Nd}3d_{3/2}$ has an additional peak on the tail of the mainline on the high binding energy side that can be associated with a shake-up process. Generally, the 3d and 4d spectral regions of the presented oxides (Fig. 4, S2–S4) are complicated by some shake-down and shake-up satellites resulting from core-hole screening effects in the final state [44]. Furthermore, the measurements with the EDX detector coupled with XPS proved the grafting of the aforementioned molecules, C6 and FC6 (Table 1).

The quantitative analysis of functionalization efficiency (E_f) has been studied with the implementation of TGA and BET methods [38,39] and determination of the number of hydroxyl groups available before and after modification (Eq. (2),3).

$$n_{\text{OH}} [\text{mmol} \cdot \text{g}^{-1}] = \frac{2[\text{WL}(T_0) - \text{WL}(T_f)]}{100 \cdot M_{\text{H}_2\text{O}}} \quad (2)$$

$$n [\text{OH} \cdot \text{m}^{-2}] = \left(\frac{2[\text{WL}(T_0) - \text{WL}(T_f)]}{100 \cdot M_{\text{H}_2\text{O}}} \right) \left(\frac{N_A}{S_{\text{BET}}} \right) \quad (3)$$

where $\text{WL}(T_0) - \text{WL}(T_f)$ stands for mass loss (wt%) in the temperature range of interest: 110–230 °C, $M_{\text{H}_2\text{O}}$ is water molar mass, N_A is Avogadro constant, and S_{BET} is the specific surface area derived from BET.

All of the investigated samples of lanthanides were grafted with high efficiency, in the range of 68–84%. There was no relation between the type of modifier and the level of efficiency (Table 2). The established data were comparable with the modification of alumina and titania with the same type of modifiers [38,39,45].

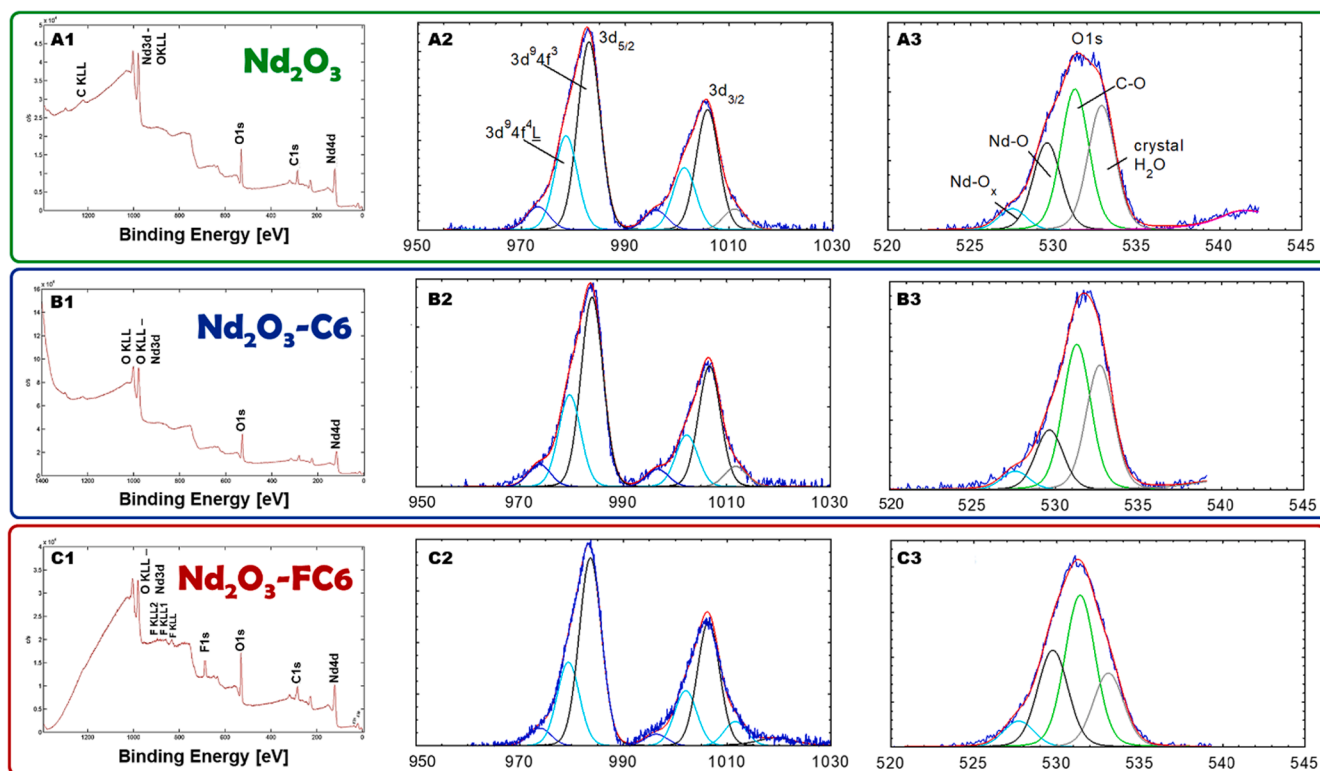


Fig. 4. XPS survey spectra of Nd_2O_3 (A1), $\text{Nd}_2\text{O}_3\text{-C6}$ (B1), and $\text{Nd}_2\text{O}_3\text{-FC6}$ (C1). High-resolution spectra of Nd_2O_3 (A2, A3), $\text{Nd}_2\text{O}_3\text{-C6}$ (B2, B3), and $\text{Nd}_2\text{O}_3\text{-FC6}$ (C2, C3).

Table 1
Elemental composition determined by XPS.

Sample	Bands and amount of elements [%]			
	Ce3d	O1s	C1s	F1s
CeO_2	32.34	67.66	–	–
$\text{CeO}_2\text{-C6}$	18.84	41.28	39.88	–
$\text{CeO}_2\text{-FC6}$	18.85	32.25	43.05	5.84
	Pr3d	O1s	C1s	F1s
Pr_6O_{11}	32.57	67.43	–	–
$\text{Pr}_6\text{O}_{11}\text{-C6}$	25.78	53.38	20.84	–
$\text{Pr}_6\text{O}_{11}\text{-FC6}$	8.60	33.03	32.34	26.03
	Nd4d	O1s	C1s	F1s
Nd_2O_3	39.57	60.43	–	–
$\text{Nd}_2\text{O}_3\text{-C6}$	26.82	40.96	32.22	–
$\text{Nd}_2\text{O}_3\text{-FC6}$	13.71	38.57	33.49	14.23
	Gd4d	O1s	C1s	F1s
Gd_2O_3	38.96	61.04	–	–
$\text{Gd}_2\text{O}_3\text{-C6}$	22.54	41.17	36.30	–
$\text{Gd}_2\text{O}_3\text{-FC6}$	16.71	26.92	25.84	30.53

3.2. Impact on material features

The analysis with HR-TEM implementation provided data compatible with other analyses. The data revealed the pure cubic phase of Gd_2O_3 (lattice parameter $a = b = c = 9.407 \text{ \AA}$ and $\alpha = \beta = \gamma = 90^\circ$) (Fig. 5A) [46]. High purity of the single-phase Gd_2O_3 was proven by observation of one-direction alignment of atomic lines [47] in Fig. 5B, as well as by XRD spectra (Fig. 6). The analysis of XRD spectra has been carried out with the crystallographic pattern for Gd_2O_3 , JPCDS: 00-043-1015.

The disappearance (crossed arrows in Fig. 6) of a few bands from the spectra was related to the covering of the particles with an organic layer and very low initial intensity (Fig. 6). As an effect of treatment with the

Table 2
The efficiency of the functionalization process.

Sample	S_{BET} [m^2 g^{-1}]	Pore diameter [\AA]	C [–]	D_{TEM} [nm]	nOH [mmol g^{-1}]	$n[\text{OH}]$ [m^{-2} $\times 10^{20}$]	E_f [%]
CeO_2	1.96	1.2 ± 0.2	2.4	72 ± 6	0.222	6.82	–
$\text{CeO}_2\text{-C6}$	1.55	1.0 ± 0.2	1.8	75 ± 8	0.067	2.05	70
$\text{CeO}_2\text{-FC6}$	1.34	1.0 ± 0.2	1.2	75 ± 6	0.070	2.15	68
Pr_6O_{11}	6.59	6.6 ± 0.4	3.5	165 ± 12	0.255	2.33	–
$\text{Pr}_6\text{O}_{11}\text{-C6}$	5.50	6.3 ± 0.4	2.8	170 ± 16	0.064	0.59	74
$\text{Pr}_6\text{O}_{11}\text{-FC6}$	4.68	6.4 ± 0.4	2.3	168 ± 15	0.061	0.56	76
Nd_2O_3	3.38	1.4 ± 0.3	2.8	85 ± 9	0.233	4.15	–
$\text{Nd}_2\text{O}_3\text{-C6}$	2.55	1.2 ± 0.3	1.5	90 ± 12	0.044	0.97	81
$\text{Nd}_2\text{O}_3\text{-FC6}$	2.03	1.2 ± 0.3	1.2	90 ± 15	0.037	0.65	84
Gd_2O_3	3.84	3.4 ± 0.3	1.7	108 ± 15	0.222	3.48	–
$\text{Gd}_2\text{O}_3\text{-C6}$	3.12	3.2 ± 0.3	1.2	110 ± 20	0.055	0.87	79
$\text{Gd}_2\text{O}_3\text{-FC6}$	2.88	3.2 ± 0.3	0.9	110 ± 20	0.049	0.78	81

silane-based modifier, no influence on the crystallographic structure was observed (Fig. 5, 7, S5, S6). The measured distance between planes was equal to 5.3 \AA in the [222] direction and 2.8 \AA in the [400] direction, respectively. The selected area diffraction (SAED) patterns were registered for the bulk of the material (Fig. 5 B1, B2) as well as for the surface of modified materials (Fig. 5 B3, B4). Differences between the bulk of the sample and the surface of modified samples have been observed, they were due to the presence of organic nanolayer with the thickness of

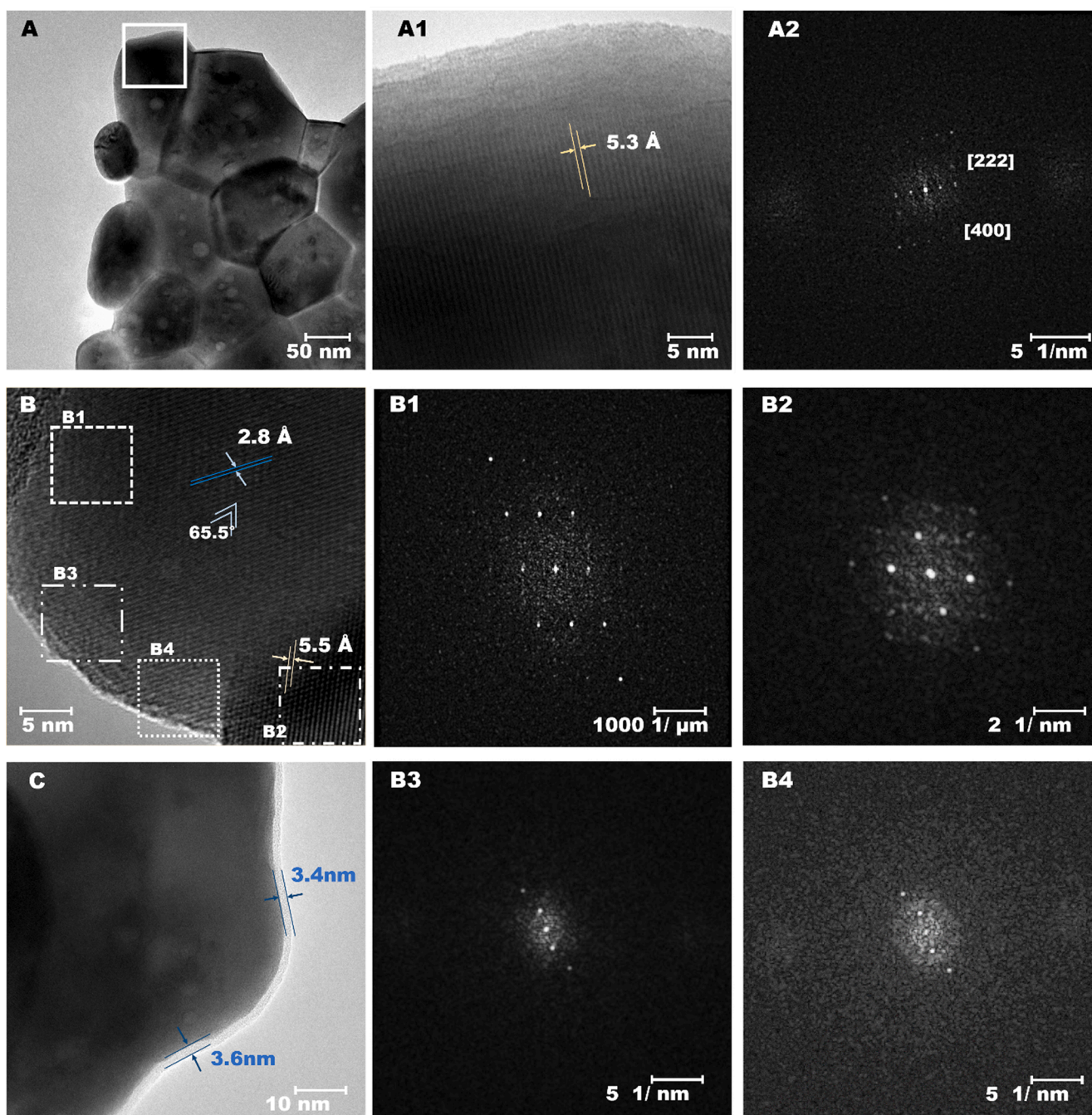


Fig. 5. TEM images - pristine Gd_2O_3 – (A, A1) and selected-area diffraction patterns (A2); for functionalized Gd_2O_3 with C6 (B, B1-B4) and FC6 (C). Selected-area diffraction patterns (bulk: B1, B2, surface: B3, B4).

around 3.5 nm (Fig. 5C). The thickness was not influenced by the type of modifier used. The generation of organic nanolayer was proven by the appearance of rings on SAED spectra (Fig. 5 B3, B4). The same tendency has been observed for other investigated oxides of lanthanides (Fig. S5 – CeO_2 , Fig. S6 – Pr_6O_{11}). In the case of Nd_2O_3 (Figs. 7, 8), the alignment of metal-to-metal lines in TEM images appeared to have different directions (Fig. 8). It was related to the co-existence of different forms of Nd_2O_3 . Indeed, XRD has revealed (Fig. 7) the characteristic bands from hexagonal phases (lattice parameter $a = b = 6.165 \text{ \AA}$, $c = 3.217 \text{ \AA}$ and $\alpha = \beta = 90^\circ$, $\gamma = 120^\circ$) trigonal ones (lattice parameter $a = b = 3.860 \text{ \AA}$, $c = 6.091 \text{ \AA}$ and $\alpha = \beta = 90^\circ$, $\gamma = 120^\circ$), and cubic ones (lattice parameter $a = b = c = 9.682 \text{ \AA}$ and $\alpha = \beta = \gamma = 90^\circ$) [48,49]. The trigonal phase was the most abundant one in the case of pristine Nd_2O_3 . However, the introduction of the functionalization process changed the phase

composition of the sample (Fig. 7). New characteristic bands for the cubic form were generated at 2theta equal to 32.02° [400] and to 50.3° [611].

Additionally, the share of hexagonal phase increased, which was proven by new bands at 2theta equal to 44.08° [021], 51.34° [030], 59.34° [031], 65.45° [112], and 80.48° [032], respectively. Similarly to the example discussed above, the presence of rings on the SAED image supports the supposition of high efficiency of grafting process (Fig. 8 B2, C2). For CeO_2 and Pr_6O_{11} , the clear dominance of one-phase material was observed (Fig. S5-S8). 93% of CeO_2 was in cubic form (lattice parameter $a = b = c = 3.866 \text{ \AA}$, and $\alpha = \beta = \gamma = 90^\circ$), while the remaining part was in tetragonal form/one (lattice parameter $a = b = 5.135 \text{ \AA}$, $c = 3.636 \text{ \AA}$, and $\alpha = \beta = \gamma = 90^\circ$) [50] (Fig. S5, S7). Praseodymium oxide was, however, mostly in triclinic phase ($a = 6.917 \text{ \AA}$, $b =$

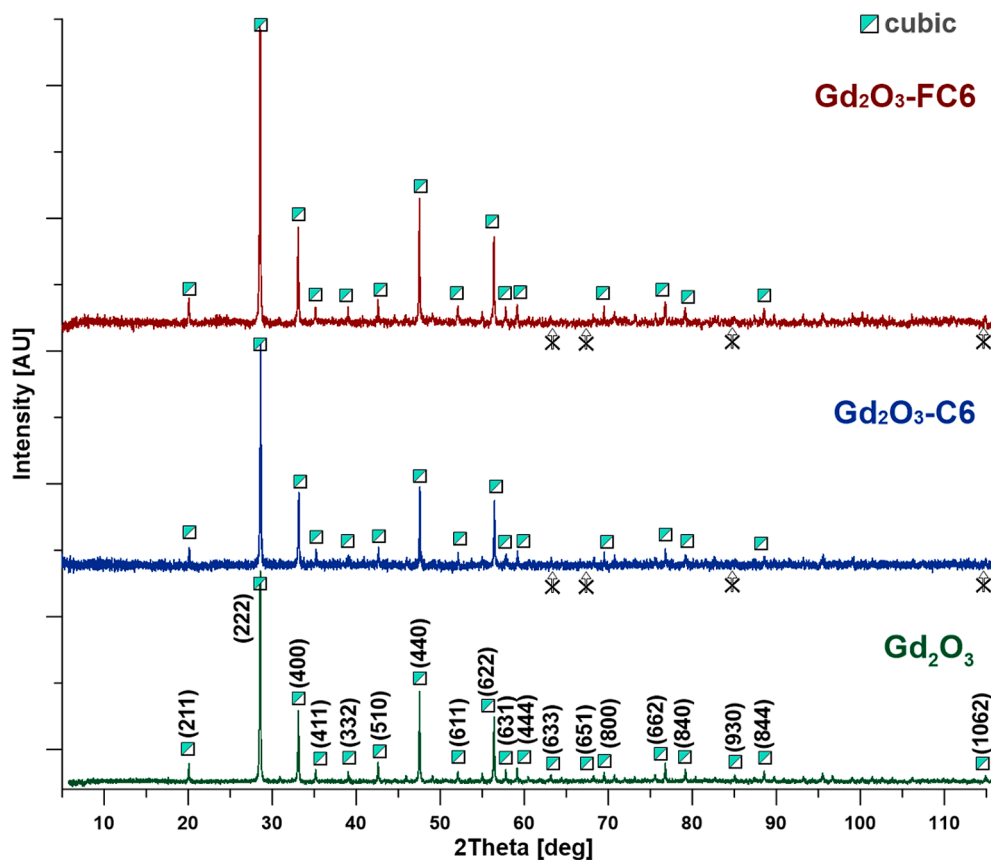


Fig. 6. XRD characteristics of pristine and functionalized lanthanide powders of Gd_2O_3 .

12.264 Å, $c = 13.453$ Å, and $\alpha = 89.097^\circ$, $\beta = 78.275^\circ$, $\gamma = 89.566^\circ$) - in 76%, with the remaining 24% in monoclinic phase ($a = 12.157$ Å, $b = 6.968$ Å, $c = 13.418$ Å, and $\alpha = 79.635^\circ$, $\beta = \gamma = 90^\circ$) [51] (Fig. S6, S8). The upkeeping of crystallographic structure of the REO after the treatment with alkylsilanes and fluoroalkylsilanes is crucial for further application of the REO in materials science and its use for engineering applications.

The TEM technique was also implemented for the analysis of the crystallite size. The measurements have been performed fifty times for each sample, using TEM images. The average sizes of the particles of pristine REO were as follows: 72 ± 6 nm (CeO_2), 165 ± 12 nm (Pr_6O_{11}), 85 ± 9 nm (Nd_2O_3), and 108 ± 15 nm (Gd_2O_3), respectively (Table 2). After functionalization, an increase of particle size by around 3–4 nm was observed, which was consistent with the size of the modifier (3.4 nm).

The reduction of specific surface area and pore diameter were other indicators for successful functionalization (Table 2). However, the reduction of C parameter (describing the equilibrium of adsorption and the degree of interaction between adsorbent and adsorbate) revealed changes not only in the textural properties of oxides of lanthanides but also in their chemistry (Table 2). A lower value of the C constant is characteristic for samples demonstrating weaker interaction with the adsorbate (nitrogen), ensuring outstanding ability to undergo chemical modification. Similar observations were reported by Knozowska et al. [45] for the hydrophobization process of alumina oxide nanopowders with the following silane-based modifiers: octyltriethoxysilane, 1H,1H,2H,2H-perfluorooctyltriethoxysilane, tetradecyltriethoxysilane, and 1H,1H,2H,2H-perfluorotetradecyltriethoxysilane. The value of parameter C for the samples decreased significantly, also a direct correlation between the value of C, hydrophobicity level of the modifiers and grafting efficiency was found.

To fulfill the requirements concerning characteristics of the material,

hydrodynamic diameter, zeta potential, and stability in the water medium of the pristine and modified REO materials were measured. The collected data are presented in Table 3. An increase of REO hydrodynamic diameter was observed for all of the investigated samples as an effect of functionalization. REO modified with non-fluorinated modifier FC6 show a more marked tendency to agglomerate than samples treated with fluorinated analogue. The above-mentioned remark can be related to the different chemical nature of the material, due to the presence or absence of fluorine, and directly to the bigger diameter of perfluorinated chains, which creates a higher energy penalty for hydration [52,53]. Furthermore, it was connected with and explained by the higher polydispersity index for the samples modified with C6. The most apparent differences were observed for CeO_2 and Gd_2O_3 , where the polydispersity index changed from 33% (CeO_2) and 29% (Gd_2O_3) for pristine material to 51% (CeO_2 -C6) and 59% (Gd_2O_3 -C6) after treatment with C6, respectively. However, functionalization with fluorine-containing a modifier changes the polydispersity index to 34% (CeO_2 -C6) and 27% (Gd_2O_3 -C6). The lower stability of C6 modified oxides can be explained by crosslinking between particles and the formation of siloxane bonds. Similar behavior was pointed out by Caputo et al. [54] during the modification of CeO_2 with 6-{2-[2-(2-methoxy-ethoxy)-ethoxy]-hexyl}triethoxysilane and 3-Aminopropyltriethoxysilane for biomedical applications. Very high stability was noticed for Pr_6O_{11} and Nd_2O_3 . The distribution of hydrodynamic diameter in water demonstrated a mono-dispersed population of ca. 1 μm (Fig. S9). The surface charge of REO materials was analyzed by zeta potential measurements in water ($pH = 5.8$). The surface charge was clearly influenced by the functionalization process (Table 3). The measured values of pristine REO were in good accordance with literature data [55]. Zeta potential depends strongly on particle size [56]. Particles with a diameter of ca. 1 μm in the aqueous medium typically carry an electric charge and have the inclination to approach one another under the Brownian movement

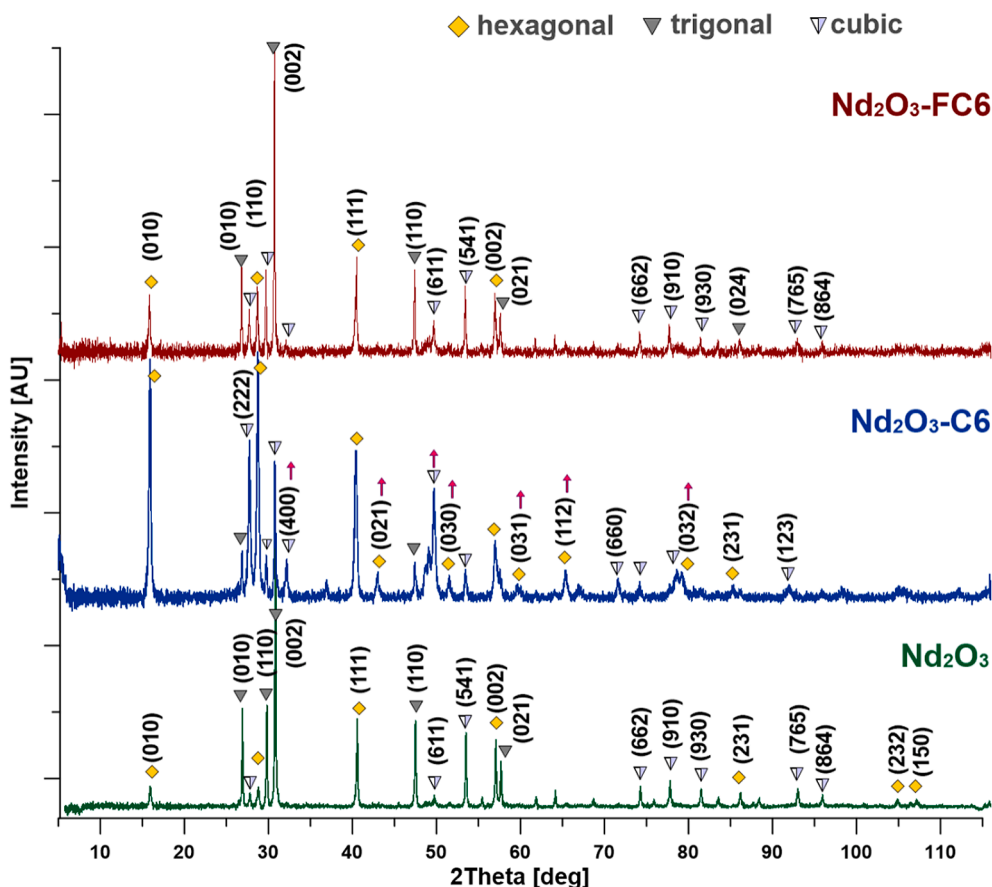


Fig. 7. XRD characteristics of pristine and functionalized lanthanide powders Nd_2O_3 .

principle [57]. On the basis of the Derjaguin-Landau-Verwey-Overbeek (DLVO) theory [58], in a situation when the kinetic energy of the colliding particles is high enough to overcome the barrier of energy from the electrostatic repulsive force, the van der Waals attractive force prevails and causes the particles to adhere strongly together. This principle applies to coagulation or flocculation, thereby increasing the size of colloidal aggregates [59]. The stability of the nanoparticles and submicron-size particles in water depends on the electrostatic or double-layer repulsive forces if only DLVO forces are available. It should be remembered that electrostatic or double-layer repulsive forces are much stronger than the van der Waals attractive forces [60]. For the range of non-DLVO attractive forces such as hydrophobic ones, bridging by adsorbed additives, patch charging and hydrogen bonding of function groups of adsorbed additives dominate [61]. The cause of the substantial difference between zeta potential for pristine and functionalized material was the introduction of alkyl and perfluoroalkyl chains, as well as introduction of higher hydrophobicity.

3.3. Impact on wettability features

The surface microstructure is another major factor that affected the features of the material, it also has a significant impact on surface hydrophobicity. As a consequence of REO functionalization with the silane-based modifiers, well-developed, heterogenic structures are generated (Fig. 9, S10). In particular, in the case of CeO_2 and Nd_2O_3 fractal-like structures have been created (Fig. 9). Such a type of microstructure plays an essential role in the hydrophobic and superhydrophobic features of materials [34].

Fractals are unique objects with a patterned structure, having self-similarity at every scale or over a range of length scales [62]. The factor characterizing a fractal structure is the fractal dimension (D), which

can have a non-integer value [63] (Eq. (4)). $(L/l)^{D-2}$ represents the roughness parameter, where L and l are upper (island-like micro-sized structures) and lower limit (sub-micrometer-sized particles) scales on the fractal surface (Fig. 9), respectively. For the lotus-like structure, L and l correspond to the dimension of the papillae and branch-like nanostructures, accordingly [63]. REO is very similar to the above-mentioned structures (Fig. 9). The important thing is that the wetting feature of fractal materials may be significantly different from that of materials with simple and ordinarily-ordered structures (even rough ones). Feng et al. [63] introduced Cassie-Baxter formalism for fractal structure, including additional fractional coverage (f_s) (Eq. (4)). This equation has excellent potential in determining fractal dimensions and the surface structure of materials by implementing contact angle (contact angle of fractal surface - θ_f) measurements and SEM imaging.

$$\cos\theta_f = f_s \left(\frac{L}{l}\right)^{D-2} \cos\theta + f_s - 1 \quad (4)$$

The values of contact angle for pristine oxides of lanthanides were in the range between 100.7° for CeO_2 and 154.8° for Pr_6O_{11} . However, the determined fractional coverage parameter was in the range from 0.18 (Pr_6O_{11}) to 0.35 ($\text{Nd}_2\text{O}_3\text{-FC6}$) (Table S1). For ceria, however, this parameter was in the range between 0.20 (CeO_2) and 0.26 ($\text{CeO}_2\text{-FC6}$), which is in close compliance with the literature data. Li and co-workers [34] found that this factor was between 0.21 and 0.28 for CeO_2 modified with 1,1,2,2-tetrahydroperfluorodecyltrimethoxysilane, by means of plasma spray-vapor deposition. The changes in the f_s parameter depended on the distance of the sample from the sprayer [34].

The high level of hydrophobicity for REO is related to its unique electron structure that prevents hydrogen bonding with water molecules. Furthermore, the high level of contact angle for water, according to literature, could be linked to hydrocarbon adsorption and airborne

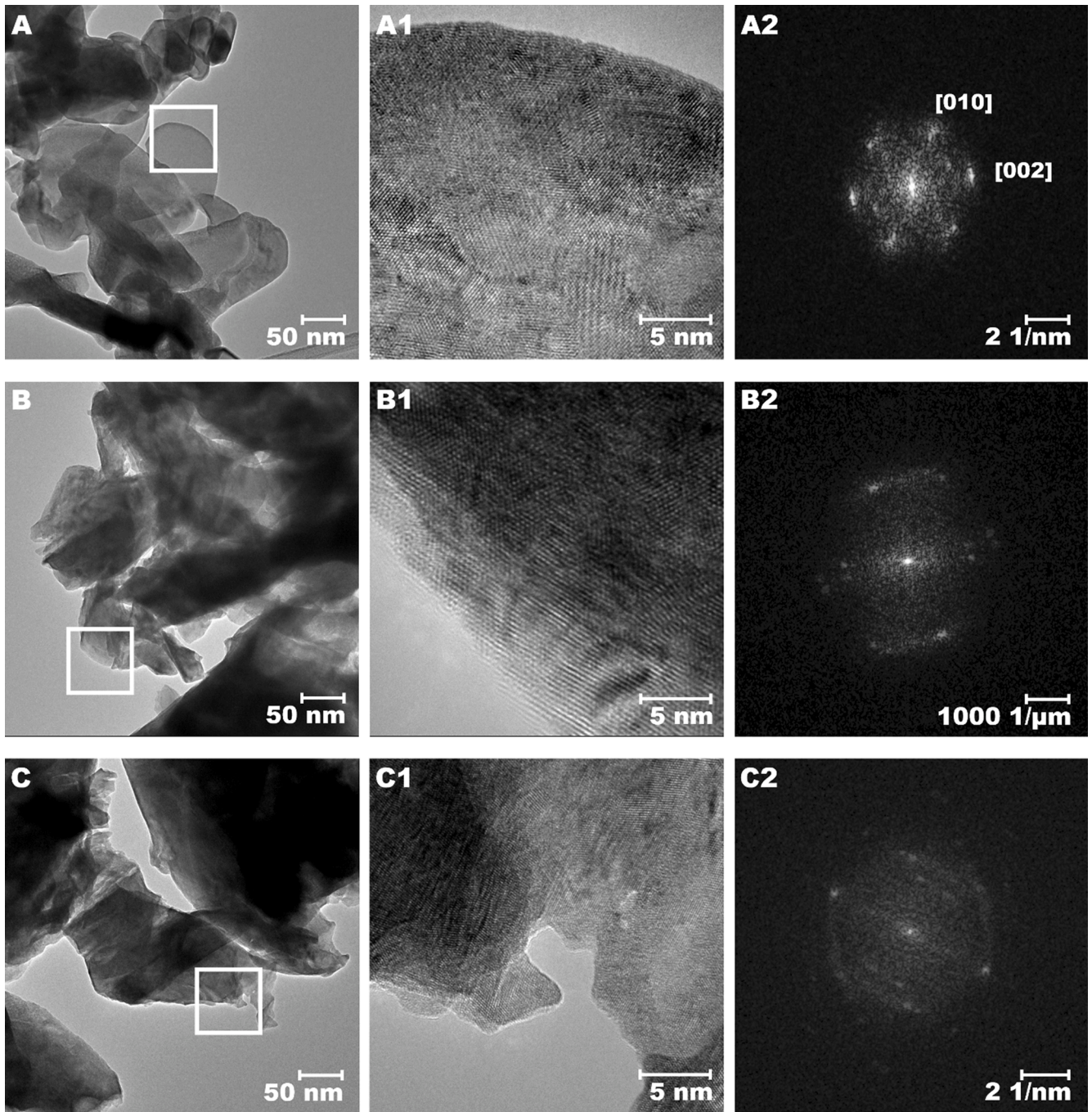


Fig. 8. TEM images - pristine Nd_2O_3 – (A, A1) and selected-area diffraction patterns (A2); functionalized Gd_2O_3 with C6 (B, B1-B4) and FC6 (C). Selected-area diffraction patterns (bulk: B1, B2, surface: B3, B4).

Table 3
DLS and ζ - zeta potential characteristics of the REO.

Sample	Hydrodynamic diameter* [nm]	Polydispersity index [%]	ζ potential* [mV]	Conductivity [mS cm ⁻¹]	Electrophoretic mobility [$\mu\text{m cm V}^{-1} \text{s}^{-1}$]
CeO ₂	340 ± 15	33%	-19.40	0.018	-1.374
CeO ₂ -C6	555 ± 26	51%	-8.26	0.061	-0.583
CeO ₂ -FC6	441 ± 20	34%	-8.97	0.073	-0.636
Pr ₆ O ₁₁	814 ± 25	27%	-7.92	0.056	-0.562
Pr ₆ O ₁₁ -C6	1267 ± 35	28%	-11.75	0.043	-0.832
Pr ₆ O ₁₁ -FC6	1217 ± 31	26%	-14.96	0.044	-1.061
Nd ₂ O ₃	866 ± 24	28%	3.04	0.028	0.215
Nd ₂ O ₃ -C6	939 ± 29	30%	17.67	0.042	1.253
Nd ₂ O ₃ -FC6	955 ± 28	26%	-0.49	0.039	-0.035
Gd ₂ O ₃	917 ± 33	29%	-14.83	0.179	-1.051
Gd ₂ O ₃ -C6	1133 ± 41	59%	-6.88	0.114	-0.487
Gd ₂ O ₃ -FC6	1035 ± 38	27%	-8.99	0.047	-0.637

* Average hydrodynamic diameter and ζ potential ± standard deviation over five measurements, obtained by cumulative analysis.

contaminants [64]. Nevertheless, the functionalized materials demonstrated an extremely high level of hydrophobicity (Fig. 10). For the samples treated with C6, the water contact angle values were between 143.5° for CeO₂-C6 and 164.8° for Gd₂O₃-C6. Materials with fractal-like structure, generated by functionalization with FC6, were characterized by contact angle from 170.5° to 175.5° for CeO₂ and Nd₂O₃, respectively. An interesting finding was the substantial reduction of the polar part of surface free energy (SFE) (Fig. 10B, Table 4). Generally, the surface free energy decreases in the sequence -CH₂ > CH₃ > -CF₂ > -CF₃ [65,66]. For the pristine material, the reduction of the polar part was associated with changes in the substance chemistry and electron occupancy. However, all modified samples revealed very low levels of the SFE polar part. In particular, treatment with FC6 enables to produce materials with that component slightly above zero (Fig. 10). Taking into account the discussion and monitoring of the adhesive feature, the work of adhesion (W_{adh}) and spreading pressure (S) were determined by Eq.5 [67,68]. S indicates the difference in the work of adhesion between phases and the work of cohesion for the phase under consideration (testing liquid). The determined value of S can be either negative (incomplete wetting) or positive (liquid penetration into the material) [67,68]. Spreading pressure levels for the investigated materials were in the range from -145.37 to -86.33 mN m⁻¹, ensuring highly hydrophobic features of all samples.

$$S = W_{1,2} - W_{1,1} \quad (5)$$

The value of the adhesive work was reduced the most significantly for CeO₂ sample, from 59.27 mN m⁻¹ (pristine CeO₂) to 1.01 mN m⁻¹ (CeO₂-FC6). However, the smallest value has been reached for Nd₂O₃ after treatment with FC6, the adhesion decreased to 0.23 mN m⁻¹.

REO modification with C6 and FC6 allows to adjust the features of materials and to change the lotus-like surface (highly hydrophobic with low adhesion) to the petal-like surface (highly hydrophobic with high adhesion). This finding is crucial from the application point of view and for the generation of non-adhesive surfaces with high resistance.

3.4. Thermal stability

During the development of a new type of material, it is crucial to define its stability and resistance under different conditions. For the research presented here, thermal features (T_{dec} - temperature decomposition) with energy effects have been studied (Table 4). Generally, oxides of lanthanides are very stable materials with melting temperatures in the range between 2183 °C (Pr₆O₁₁) and 2420 °C (Gd₂O₃). For this reason, it was only possible to analyze the characteristics of the grafted layer in the course of TGA analysis (Table 4). In the case of pristine materials, the changes in the mass were related to the removal of water from the ceramic structure (Table 4, Fig. 11). Improvement of thermal stability was observed for the modified samples, regardless of the type of grafting molecules. On the other hand, the impact of ceramic support on energy features has been observed. Namely, for trivalent REO

materials, higher values of enthalpy were found for the materials grafted with C6 molecules than for FC6, which can be explained by the higher value of the surface energy for CH than for CF [65,66]. For the same reason, specific heat capacity (C_p) was also higher for alkylsilane modification. An increase of C_p was related to the higher demand for heat needed for the decomposition of the material. The most important outcome was that functionalized samples are stable in high temperatures above 280 °C, ensuring stability and usability for a long time in a broad range of applications. For instance, the prepared materials can be used as fillers applied to separation materials, they also allow to modify properties of materials.

3.5. Impact on the magnetic properties

The pristine and modified Gd₂O₃ samples show typical EPR spectra for undiluted gadolinium(III) compounds. These reveal as very broad unclosed, almost isotropic line (Fig. 12) with the following parameters: $g_{iso} \sim 2.0$, ΔB_{pp} ca. 280 mT and mixed Lorentzian-Gaussian shape. The only difference is connected with the intensities due to various concentrations of paramagnetic centers in the samples. The pristine CeO₂ sample show a rather unexpected EPR spectrum (Fig. S12). Because cerium (IV) is diamagnetic, and the line is very narrow (ΔB_{pp} ca. 0.4 mT) and located at $g = 1.962$, it probably comes from a small amount of radical impurities of unknown nature. Radical signals disappear after functionalization with C6 or FC6. All other samples i.e. Nd₂O₃, Nd₂O₃-C6, Nd₂O₃-FC6, Pr₆O₁₁, Pr₆O₁₁-C6, and Pr₆O₁₁-FC6 are EPR inactive. The functionalization process with 1H,1H,2H,2H-perfluorooctyltriethoxysilane (FC6) and n-octyltriethoxysilane (C6) have not been generated radicals on the surface of the studied lanthanide oxides. The most important and valuable result was the fact that after the modification process, the material maintains its magnetic properties. The introduction of functionalizing nanolayer tunes the wettability, roughness, and chemistry of the materials, however the magnetic features were unchanged. The presented statement has a vast implication in the material applicability.

4. Conclusions

The unique properties of the selected rare earth oxides were taken into consideration in the generation of a new type of hybrid materials. According to the presented method, the material feature from the petal effect to lotus one was switched in a single-step process. Functionalization with two types of silanes-based modifiers was characterized by high effectiveness between 67 and 84%. The element of novelty was an efficient modification of REO (CeO₂, Pr₆O₁₁, Nd₂O₃, and Gd₂O₃) by chemical, covalent modification causing superhydrophobicity, low-adhesive features, and fractal-like morphology. The level of hydrophobicity was raised up to 175.5° for Nd₂O₃-FC6. The comprehensive characterization of the materials, including e.g. spectroscopic, microscopic, and goniometric methods, revealed that no influence upon their

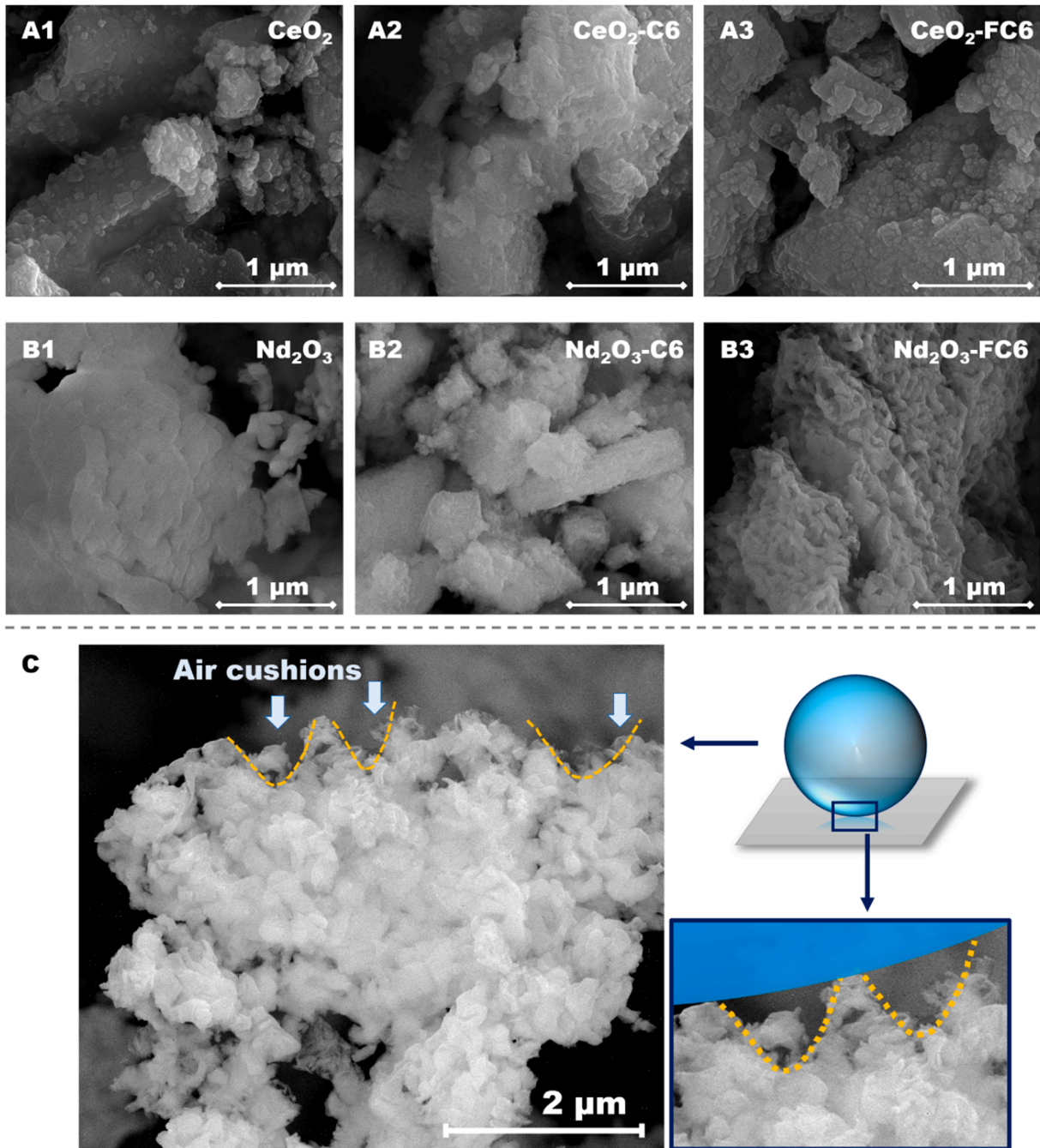


Fig. 9. SEM images of the investigated samples: CeO₂ (A1, A2, A3), Nd₂O₃ (B1, B2, B3). Pristine material (A1, B1), modified by C6 (A2, B2), and modified with FC6 (A3, B3). C - Morphology of Nd₂O₃-FC6 surface and effect of surface structure on super-hydrophobic material with fractal features.

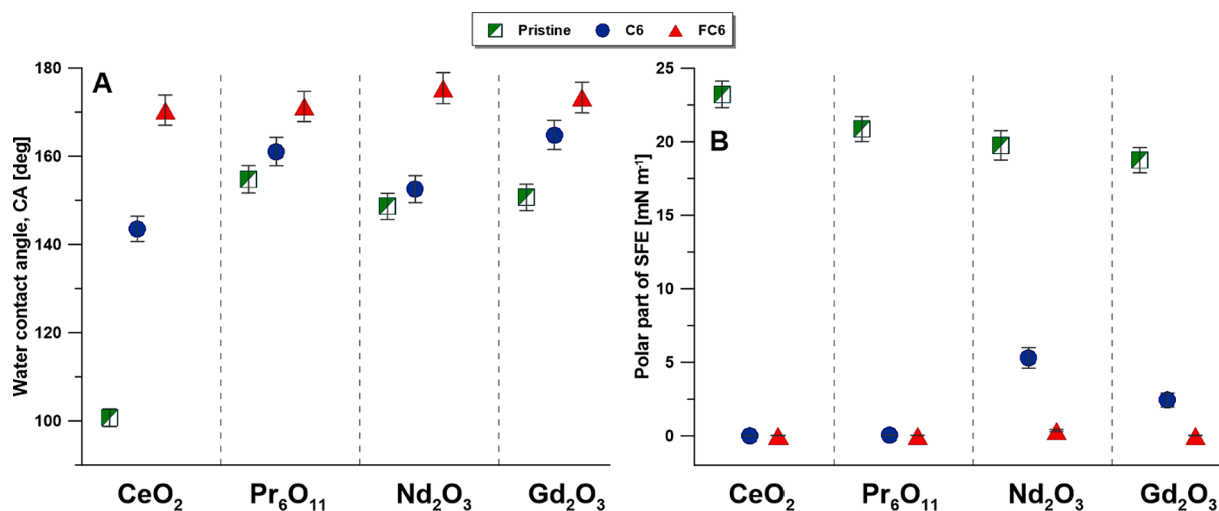


Fig. 10. Evolution of contact angle (A) and the polar component of surface free energy of pristine and modified REO.

Table 4
Thermal (TGA) and energy (DSC) features.

Sample	T _{dec} [°C]	Enthalpy [J g ⁻¹]	C _p - specific heat capacity [Jg ⁻¹ K ⁻¹]
CeO ₂	–	114.5 ± 3.4	0.155 ± 0.014
CeO ₂ -C6	362.1	167.4 ± 4.7	0.675 ± 0.018
CeO ₂ -FC6	384.1	282.7 ± 8.4	0.655 ± 0.020
Pr ₆ O ₁₁	271.1	390.2 ± 11.4	6.479 ± 0.133
Pr ₆ O ₁₁ -C6	288.1	420.1 ± 13.2	6.416 ± 0.140
Pr ₆ O ₁₁ -FC6	283.0	231.7 ± 9.4	3.197 ± 0.104
Nd ₂ O ₃	298.9	933.1 ± 11.4	4.128 ± 0.111
Nd ₂ O ₃ -C6	315.2	831.1 ± 15.8	2.661 ± 0.150
Nd ₂ O ₃ -FC6	302.5	503.6 ± 7.1	2.084 ± 0.124
Gd ₂ O ₃	–	68.27 ± 5.4	1.476 ± 0.104
Gd ₂ O ₃ -C6	306.3	205.4 ± 2.4	2.319 ± 0.167
Gd ₂ O ₃ -FC6	316.2	44.97 ± 1.8	1.208 ± 0.045

crystallographic and magnetic properties was noticed. The presented method allows preparing stable materials with a high potential in materials chemistry and modulation of surface features. These materials

could be useful as coatings at large scales using a wide diversity of ceramic processing techniques. The presented material and developed method will help comprehend the industrial and scientific potential of hydrophobic surfaces by addressing some crucial aspects of robustness. The modified powders with the presented feature can be also applied in heat transfer fluids, enhancing the heat convection and thermal conductivity.

CRediT authorship contribution statement

Joanna Kujawa: Conceptualization, Methodology, Resources, Data curation, Writing - original draft, Writing - review & editing, Visualization, Supervision, Project administration, Funding acquisition. **Samer Al-Gharabli:** Methodology, Writing - original draft, Writing - review & editing. **Grzegorz Wrzeszcz:** Investigation, Writing - original draft, Writing - review & editing. **Katarzyna Knozowska:** Investigation, Writing - review & editing, Visualization. **Renars Lagzdins:** Data curation, Writing - review & editing. **Ewa Talik:** Investigation, Data curation, Writing - review & editing. **Arkadiusz Dzedzic:** Writing - review & editing. **Patrick Loulergue:** Writing - review & editing.

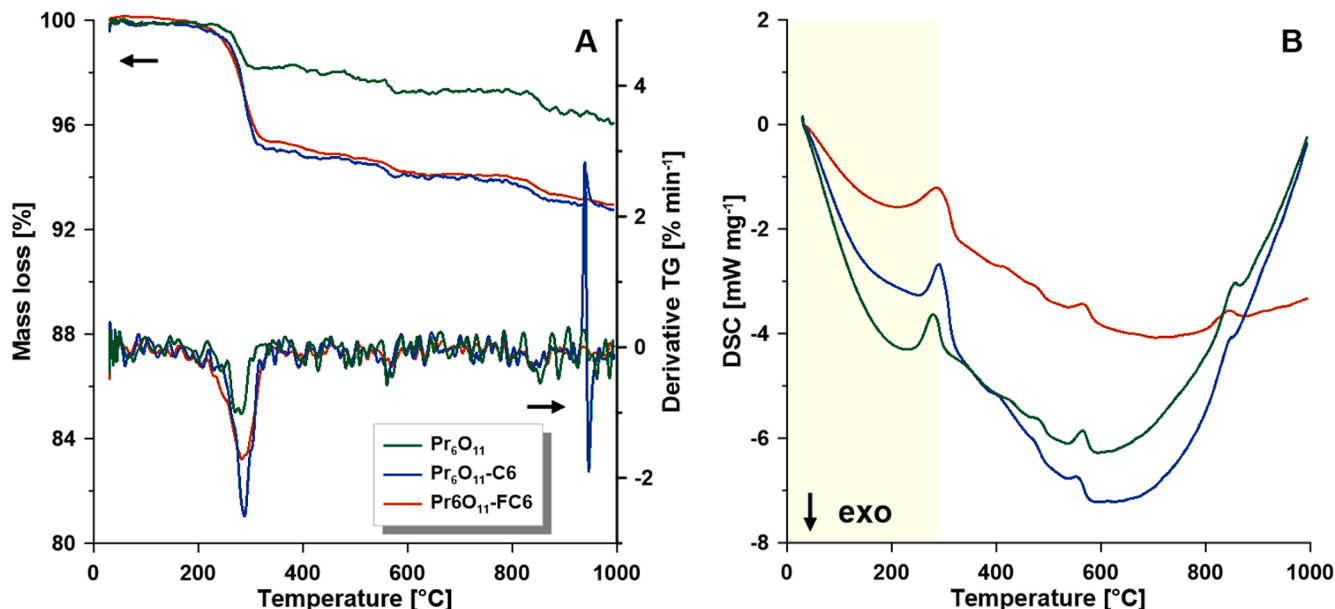


Fig. 11. Thermogravimetric analysis with 1st derivative (A) and DSC (B) for pristine and modified Pr₆O₁₁.

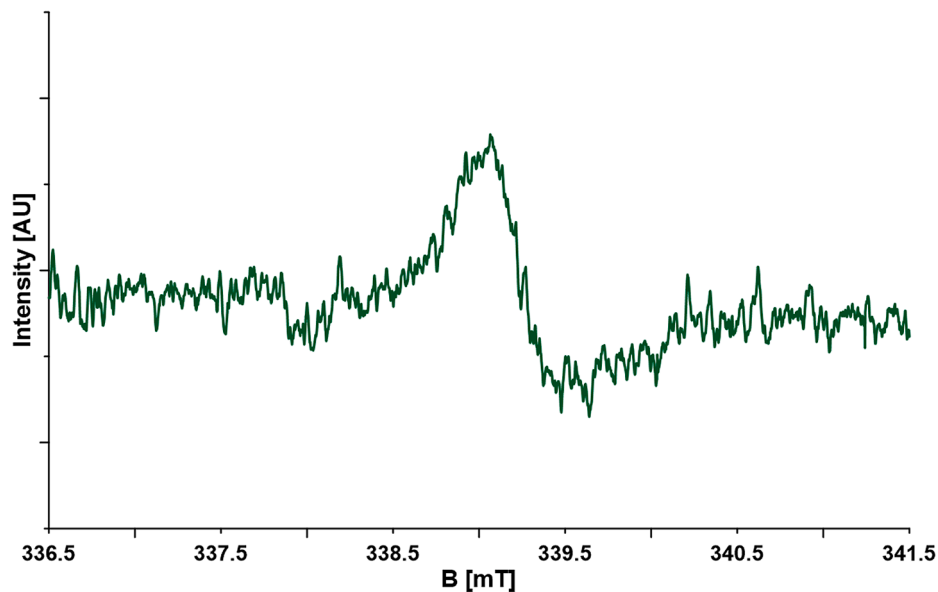


Fig. 12. EPR. X-band (9.31775 GHz) EPR spectrum of powdered pristine CeO₂ sample at room temperature.

Anthony Szymczyk: Writing - review & editing. **Wojciech Kujawski:** Validation, Resources, Writing - original draft, Writing - review & editing, Supervision.

Declaration of Competing Interest

The authors declare that they have no known competing financial interests or personal relationships that could have appeared to influence the work reported in this paper.

Acknowledgment

The research was supported by 2017/26/D/ST4/00752 (Sonata 13) grant from the National Science Centre, Poland. The research was also partly supported by the Franco-Polish Hubert Curien's Partnership Program "Polonium" PPN/BIL/2018/1/00222 - CAMPUS France PHC Polonium 2019 (n°42903VH).

Appendix A. Supplementary material

Supplementary data to this article can be found online at <https://doi.org/10.1016/j.apsusc.2020.148563>.

References

- [1] M. Liu, S. Wang, L. Jiang, Nature-inspired superwettability systems, *Nat. Rev. Mater.* 2 (2017) 17036.
- [2] S. Wang, K. Liu, X. Yao, L. Jiang, Bioinspired surfaces with superwettability: new insight on theory, design, and applications, *Chem. Rev.* 115 (2015) 8230–8293.
- [3] W. Barthlott, T. Schimmel, S. Wiersch, K. Koch, M. Brede, M. Barczewski, S. Walheim, A. Weis, A. Kaltenmaier, A. Leder, H.F. Bohn, The Salvinia Paradox: Superhydrophobic Surfaces with Hydrophilic Pins for Air Retention Under Water, *Adv. Mater.* 22 (2010) 2325–2328.
- [4] L. Feng, Y. Zhang, J. Xi, Y. Zhu, N. Wang, F. Xia, L. Jiang, Petal Effect: A Superhydrophobic State with High Adhesive Force, *Langmuir* 24 (2008) 4114–4119.
- [5] K. Autumn, Y.A. Liang, S.T. Hsieh, W. Zesch, W.P. Chan, T.W. Kenny, R. Fearing, R. J. Full, Adhesive force of a single gecko foot-hair, *Nature* 405 (2000) 681–685.
- [6] B.N.J. Persson, Wet adhesion with application to tree frog adhesive toe pads and tires, *J. Phys. Condens. Matter* 19 (2007), 376110.
- [7] M. Ahmad, M. Casey, N. Sürken, Experimental assessment of droplet impact erosion resistance of steam turbine blade materials, *Wear* 267 (2009) 1605–1618.
- [8] D. Zhang, L. Wang, H. Qian, X. Li, Superhydrophobic surfaces for corrosion protection: a review of recent progresses and future directions, *J. Coat. Technol. Res.* 13 (2016) 11–29.
- [9] Y.-Y. Quan, L.-Z. Zhang, R.-H. Qi, R.-R. Cai, Self-cleaning of Surfaces: the Role of Surface Wettability and Dust Types, *Sci. Rep.* 6 (2016) 38239.
- [10] S.K. Sethi, G. Manik, Recent progress in super hydrophobic/hydrophilic self-cleaning surfaces for various industrial applications: a review, *Polym. Plast. Technol. Eng.* 1–21 (2018).
- [11] A.H.C. Ng, R. Fobel, C. Fobel, J. Lamanna, D.G. Rackus, A. Summers, C. Dixon, M. D.M. Dryden, C. Lam, M. Ho, N.S. Mufti, V. Lee, M.A.M. Asri, E.A. Sykes, M. D. Chamberlain, R. Joseph, M. Ope, H.M. Scobie, A. Knipes, P.A. Rota, N. Marano, P.M. Chege, M. Njuguna, R. Nzunza, N. Kisangau, J. Kiogora, M. Karungi, J. W. Burton, P. Borus, E. Lam, A.R. Wheeler, A digital microfluidic system for serological immunoassays in remote settings, *Sci. Transl. Med.* 10 (2018).
- [12] T.L. Liu, C.-J.C. Kim, Turning a surface superrepellent even to completely wetting liquids, *Science* 346 (2014) 1096–1100.
- [13] K. Golovin, A. Tuteja, A predictive framework for the design and fabrication of icephobic polymers, *Sci. Adv.* 3 (2017).
- [14] M. Li, G. Qing, Y. Xiong, Y. Lai, T. Sun, CH- π Interaction Driven Macroscopic Property Transition on Smart Polymer Surface, *Sci. Rep.* 5 (2015) 15742.
- [15] P. Cataldi, I.S. Bayer, R. Cingolani, S. Marras, R. Chellali, A. Athanassiou, A thermochromic superhydrophobic surface, *Sci. Rep.* 6 (2016) 27984.
- [16] J. Kujawa, S. Al-Gharabli, W. Kujawski, K. Knozowska, Molecular grafting of fluorinated and nonfluorinated alkylsiloxanes on various ceramic membrane surfaces for the removal of volatile organic compounds applying vacuum membrane distillation, *ACS Appl. Mater. Interfaces* 9 (2017) 6571–6590.
- [17] M. Badv, I.H. Jaffer, J.I. Weitz, T.F. Didar, An omniphobic lubricant-infused coating produced by chemical vapor deposition of hydrophobic organosilanes attenuates clotting on catheter surfaces, *Sci. Rep.* 7 (2017) 11639.
- [18] S. Dirè, D. Bottone, E. Callone, D. Maniglio, I. Génois, F. Ribot, Hydrophobic coatings by thiol-ene click functionalization of silsesquioxanes with tunable architecture, *Mater.* 10 (2017) 913.
- [19] P. Champathet, V. Ervithayasuporn, T. Osotchan, S. Dangtip, Hydrophobic thiol-ene surfaces fabricated via plasma activation and photo polymerization, *J. Phys. Conf. Ser.* 901 (2017), 012164.
- [20] H. Sai, K.W. Tan, K. Hur, E. Asenath-Smith, R. Hovden, Y. Jiang, M. Riccio, D. A. Muller, V. Elser, L.A. Estroff, S.M. Gruner, U. Wiesner, Hierarchical porous polymer scaffolds from block copolymers, *Science* 341 (2013) 530–534.
- [21] G. Azimi, Y. Cui, A. Sabanska, K.K. Varanasi, Scale-resistant surfaces: Fundamental studies of the effect of surface energy on reducing scale formation, *Appl. Surf. Sci.* 313 (2014) 591–599.
- [22] Y. Tian, L. Jiang, Intrinsically robust hydrophobicity, *Nature Mat.* 12 (2013) 291.
- [23] S. Khan, G. Azimi, B. Yildiz, K.K. Varanasi, Role of surface oxygen-to-metal ratio on the wettability of rare-earth oxides, *Appl. Phys. Lett.* 106 (2015).
- [24] G. Azimi, R. Dhiman, H.-M. Kwon, A.T. Paxson, K.K. Varanasi, Hydrophobicity of rare-earth oxide ceramics, *Nature Mat.* 12 (2013) 315.
- [25] J. Tam, G. Palumbo, U. Erb, G. Azimi, Robust hydrophobic rare earth oxide composite electrodeposits, *Adv. Mater. Inter.* 4 (2017) 1700850.
- [26] I.-K. Oh, K. Kim, Z. Lee, K.Y. Ko, C.-W. Lee, S.J. Lee, J.M. Myung, C. Lansalot-Matras, W. Noh, C. Dussarrat, H. Kim, H.-B.-R. Lee, Hydrophobicity of rare earth oxides grown by atomic layer deposition, *Chem. Mater.* 27 (2015) 148–156.
- [27] S.-P. Fu, J. Rossero, C. Chen, D. Li, C.G. Takoudis, J.T. Abiade, On the wetting behavior of ceria thin films grown by pulsed laser deposition, *Appl. Phys. Lett.* 110 (2017), 081601.
- [28] Q. Lv, S. Zhang, S. Deng, Y. Xu, G. Li, Q. Li, Y. Jin, Transparent and water repellent ceria film grown by atomic layer deposition, *Surf. Coat. Technol.* 320 (2017) 190–195.
- [29] D.J. Preston, N. Miljkovic, J. Sack, R. Enright, J. Queeney, E.N. Wang, Effect of hydrocarbon adsorption on the wettability of rare earth oxide ceramics, *Appl. Phys. Lett.* 105 (2014), 011601.

- [30] J. Tam, B. Feng, Y. Ikuhara, H. Ohta, U. Erb, Crystallographic orientation–surface energy–wetting property relationships of rare earth oxides, *J. Mater. Chem. A* 6 (2018) 18384–18388.
- [31] D. Chandler, Interfaces and the driving force of hydrophobic assembly, *Nature* 437 (2005) 640.
- [32] N. Giovambattista, P.G. Debenedetti, P.J. Rossky, Enhanced surface hydrophobicity by coupling of surface polarity and topography, *Langmuir* 15 (1999) 15181–15185.
- [33] R. Lundy, C. Byrne, J. Bogan, K. Nolan, M.N. Collins, E. Dalton, R. Enright, Exploring the role of adsorption and surface state on the hydrophobicity of rare earth oxides, *ACS Appl. Mater. Interfaces* 9 (2017) 13751–13760.
- [34] J. Li, C.-X. Li, Q.-Y. Chen, J.-T. Gao, J. Wang, G.-J. Yang, C.-J. Li, Super-hydrophobic surface prepared by lanthanide oxide ceramic deposition through PS-PVD process, *J. Therm. Spray Technol.* 26 (2017) 398–408.
- [35] M. Sheikh, M. Pazirofteh, M. Dehghani, M. Asghari, M. Rezakazemi, C. Valderrama, J.-L. Cortina, Application of ZnO nanostructures in ceramic and polymeric membranes for water and wastewater technologies: A review, *Chem. Eng. J.* 123475 (2019).
- [36] L. Shen, Z. Huang, Y. Liu, R. Li, Y. Xu, G. Jakaj, H. Lin, Polymeric membranes incorporated with ZnO nanoparticles for membrane fouling mitigation: a brief review, *Front. Chem.* 8 (2020).
- [37] B. Soltani, M. Asghari, Effects of ZnO nanoparticle on the gas separation performance of polyurethane mixed matrix membrane, *Membranes* 7 (2017) 43.
- [38] J. Kujawa, W. Kujawski, S. Koter, A. Rozicka, S. Cerneaux, M. Persin, A. Larbot, Efficiency of grafting of Al₂O₃, TiO₂ and ZrO₂ powders by perfluoroalkylsilanes, *Colloids Surf. A* 420 (2013) 64–73.
- [39] J. Kujawa, S. Cerneaux, W. Kujawski, Characterization of the surface modification process of Al₂O₃, TiO₂ and ZrO₂ powders by PFAS molecules, *Colloids Surf. A* 447 (2014) 14–22.
- [40] A.B.D. Cassie, S. Baxter, Wettability of porous surfaces, *Trans. Faraday Soc.* 40 (1944) 546–551.
- [41] H. Tamura, K. Mita, A. Tanaka, M. Ito, Mechanism of hydroxylation of metal oxide surfaces, *J. Colloid Interf. Sci.* 243 (2001) 202–207.
- [42] J. Kujawa, W. Kujawski, Functionalization of ceramic metal oxide powders and ceramic membranes by perfluoroalkylsilanes and alkylsilanes possessing different reactive groups: physicochemical and tribological properties, *ACS Appl. Mater. Interfaces* 8 (2016) 7509–7521.
- [43] A. Guzik, E. Talik, A. Pajczkowska, S. Turczyński, J. Kusz, Magnetic properties of manganese doped PrAlO₃ monocrystalline fibres, *Mater. Sci.-Poland* 32 (2014) 633.
- [44] J.P. Baltrus, M.J. Keller, Rare earth oxides Eu₂O₃ and Nd₂O₃ analyzed by XPS, *Surf. Sci. Spectra* 26 (2019), 014001.
- [45] K. Knozowska, G. Li, W. Kujawski, J. Kujawa, Novel heterogeneous membranes for enhanced separation in organic-organic pervaporation, *J. Membr. Sci.* 599 (2020), 117814.
- [46] N. Dhananjaya, H. Nagabhushana, B.M. Nagabhushana, B. Rudraswamy, S. C. Sharma, D.V. Sunitha, C. Shivakumara, R.P.S. Chakradhar, Effect of different fuels on structural, thermo and photoluminescent properties of Gd₂O₃ nanoparticles, *Spectrochim. Acta A* 96 (2012) 532–540.
- [47] D.A. Zatsepin, D.W. Boukhvalov, A.F. Zatsepin, Y.A. Kuznetsova, M. A. Mashkovtsev, V.N. Rychkov, V.Y. Shur, A.A. Esin, E.Z. Kurmaev, Electronic structure, charge transfer, and intrinsic luminescence of gadolinium oxide nanoparticles: Experiment and theory, *Appl. Surf. Sci.* 436 (2018) 697–707.
- [48] Y. Ozawa, Y. Tochiwara, A. Watanabe, M. Nagai, S. Omi, Stabilizing effect of Nd₂O₃, La₂O₃ and ZrO₂ on Pt-PdO/Al₂O₃ during catalytic combustion of methane, *Appl. Catal. A* 258 (2004) 261–267.
- [49] B. Savova, D. Filkova, D. Crişan, M. Crişan, M. Răileanu, N. Drăgan, A. Galtayries, J.C. Védrine, Neodymium doped alkaline-earth oxide catalysts for propane oxidative dehydrogenation. Part I. Catalyst characterisation, *Appl. Catal. A* 359 (2009) 47–54.
- [50] P. Tamizhdurai, S. Sakthianathan, S.-M. Chen, K. Shanthi, S. Sivasanker, P. Sangeetha, Environmentally friendly synthesis of CeO₂ nanoparticles for the catalytic oxidation of benzyl alcohol to benzaldehyde and selective detection of nitrite, *Sci. Rep.* 7 (2017) 46372.
- [51] M. Shamshi Hassan, M. Shaheer Akhtar, K.-B. Shim, O.B. Yang, Morphological and electrochemical properties of crystalline praseodymium oxide nanorods, *Nanoscale Res. Lett.* 5 (2010) 735.
- [52] V.H. Dalvi, P.J. Rossky, Molecular origins of fluorocarbon hydrophobicity, *P. Natl. Acad. Sci.* 107 (2010) 13603–13607.
- [53] G. Soliveri, V. Pifferi, R. Annunziata, L. Rimoldi, V. Aina, G. Cerrato, L. Falciola, G. Cappelletti, D. Meroni, Alkylsilane-SiO₂ hybrids. A concerted picture of temperature effects in vapor phase functionalization, *J. Phys. Chem. C* 119 (2015) 15390–15400.
- [54] F. Caputo, M. Mamei, A. Sienkiewicz, S. Licocchia, F. Stellacci, L. Ghibelli, E. Traversa, A novel synthetic approach of cerium oxide nanoparticles with improved biomedical activity, *Sci. Rep.* 7 (2017) 4636.
- [55] S. Barany, K. Bohacs, I. Chepurna, R. Meszaros, Electrokinetic properties and stability of cerium dioxide suspensions, *RSC Adv.* 6 (2016) 69343–69351.
- [56] L.B.T. La, Y.-K. Leong, H.P. Watts, P.-I. Au, K.J. Hayward, L.-C. Zhang, A novel approach for the preparation of nanosized Gd₂O₃ structure: The influence of surface force on the morphology of ball milled particles, *Colloids Surf. A* 506 (2016) 13–19.
- [57] H. Zhang, J.F. Banfield, Interatomic Coulombic interactions as the driving force for oriented attachment, *CrystEngComm* 16 (2014) 1568–1578.
- [58] H.K. Christenson, DLVO (Derjaguin–Landau–Verwey–Overbeek) theory and solvation forces between mica surfaces in polar and hydrogen-bonding liquids, *J. Chem. Soc.* 80 (1984) 1933–1946.
- [59] Y.K. Leong, B.C. Ong, Critical zeta potential and the Hamaker constant of oxides in water, *Powder Technol.* 134 (2003) 249–254.
- [60] Y.D. Liu, H.J. Choi, Electrorheological fluids: smart soft matter and characteristics, *Soft Matter* 8 (2012) 11961–11978.
- [61] Y.-K. Leong, B.-C. Ong, Polyelectrolyte-mediated interparticle forces in aqueous suspensions: Molecular structure and surface forces relationship, *Chem. Eng. Res. Des.* 101 (2015) 44–55.
- [62] Q. Zeng, Size matching effect on Wenzel wetting on fractal surfaces, *Results Phys.* 10 (2018) 588–593.
- [63] L. Feng, S. Li, Y. Li, H. Li, L. Zhang, J. Zhai, Y. Song, B. Liu, L. Jiang, D. Zhu, Super-hydrophobic surfaces: from natural to artificial, *Adv. Mater.* 14 (2002) 1857–1860.
- [64] Z. Li, Y. Wang, A. Kozbial, G. Shenoy, F. Zhou, R. McGinley, P. Ireland, B. Morganstein, A. Kunkel, S.P. Surwade, L. Li, H. Liu, Effect of airborne contaminants on the wettability of supported graphene and graphite, *Nat. Mater.* 12 (2013) 925–931.
- [65] A. Das, T.A. Farnham, S. Bengaluru Subramanyam, K.K. Varanasi, Designing ultra-low hydrate adhesion surfaces by interfacial spreading of water-immiscible barrier films, *ACS Appl. Mater. Interfaces* 9 (2017) 21496–21502.
- [66] R. Sukamanchi, D. Mathew, S. Kumar K.S, Durable Superhydrophobic Particles Mimicking Leafhopper Surface: Superoleophilicity and Very Low Surface Energy, *ACS Sustain. Chem. Eng.*, 5 (2017) 252–260.
- [67] J.J. Bikerman, The Nature of the equilibrium spreading pressure, *Kolloid. Z. Z. Polym.* 191 (1963) 33–35.
- [68] R.J. Good, Spreading pressure and contact angle, *J. Colloid Interf. Sci.* 52 (1975) 308–313.